



Running-in Period During Sliding Wear of Austenitic Steels

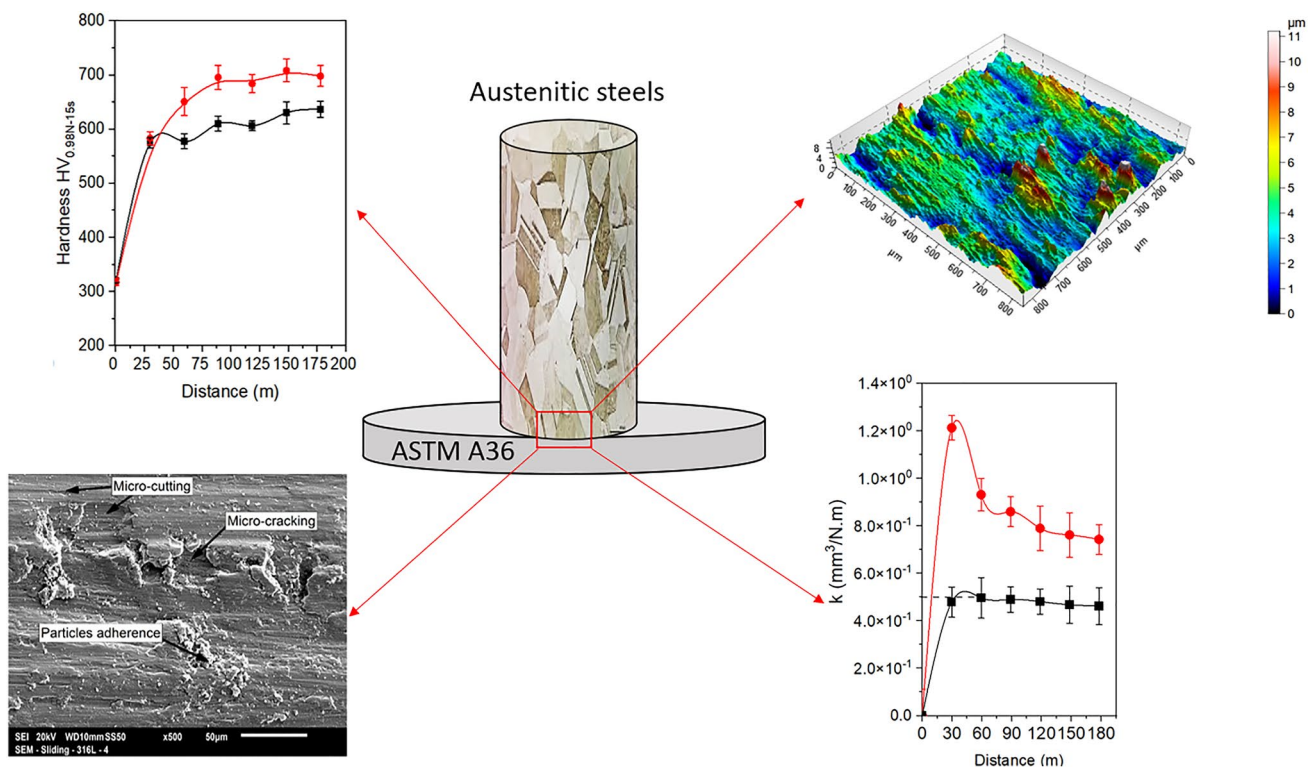
O. A. Zambrano¹ · B. Iglesias-Guerrero² · S. A. Rodríguez² · J. J. Coronado²

Received: 23 March 2024 / Accepted: 1 May 2024 / Published online: 28 May 2024
© Crown 2024

Abstract

The running-in period during dry sliding wear might determine the evolution to steady-state wear behaviour. To this end, the running-in period during sliding wear of austenitic stainless steel, AISI 316L stainless steel, and Hadfield steel were studied through the testing pin (flat-ended)-on-disk configuration. The effects of the normal load, sliding speed, and alloy type were assessed, and the specific wear rate and strain hardening characteristics were determined. The wear rate was correlated with wear mechanism, friction coefficient, hardening, and roughness to characterize the changes occurring during the running-in period. These changes could influence the responses of these materials to wear during the steady-state period. The stabilization of the specific wear rate and hardness was noted to align with the end of the running-in period.

Graphical Abstract



Keywords Running-in · Sliding wear · Roughness · Strain hardening · Friction coefficient · Austenitic steels

1 Introduction

When plotting a mass loss curve as a function of distance travelled for two surfaces in sliding contact, three characteristic regions of the curves with different stages are present: (i) the initial region known as the running-in period, (ii) the second region known as the steady period, and (iii) the last region known as the wear-out period. This behaviour occurs at the laboratory level and in industrial components. The running-in period is related to all the processes that occur before steady state is achieved, and these processes are usually accompanied by a wear rate change [1] or a friction coefficient change [2]. Conversely, this period can affirm that the steady-state regime occurs when the friction coefficient, wear rate, and surface roughness reach relatively constant levels. Despite the importance of the running-in period in machine elements that present sliding wear, such as piston rings with cylinders, bearings, and gears, few scholars have discussed this phenomenon [3–12]. Khonsari et al. [3] conducted a literature review and highlighted that the steady-state period has received significantly more attention than the running-in period. Argatov et al. [13] developed a macroscale approximation of the wear process during the running-in period. The scholars used the theory of elasticity and Archard's equation of wear to formulate the wear contact problem. Simple closed-form approximations for the running-in period and sliding distance were provided in that paper. These approximations can be useful for estimating the running-in period in wear, but further experimental validation is needed. By using a pin-on-disk test rig configuration featuring pins made of hardened steel and disks made of St37 steel, Ghatrehsamani et al. [11] showed that the transient behaviour during the running-in period is significantly influenced by the loading conditions. When the steady-state period begins, the surface roughness, wear coefficient, and friction coefficient all plateau. In other words, the loading condition during the running-in period has a significant impact on the behaviour of the system. Later, the same authors [14] claimed to have developed a model that can predict the variations in wear rate, friction coefficient, and surface asperities during running-in and validated their experiments. Recently, Ding et al. [15] studied the running-in behaviour of 7075 aluminium alloy during a burnishing process through a reciprocating tribometer. The scholars introduced a quantitative parameter d_{\max} to study the running-in period. This parameter is defined as the maximum distance between phase points, and it is introduced as a metric to quantify the extent of the phase trajectory. The magnitude of d_{\max} serves as an indicator of the phase trajectory's convergence. Notably, these discussions are framed within the

context of Takens' Theorem (1981), also referred to as the phase space reconstruction theory. This theorem is a mathematical framework that facilitates the comprehension of complex systems, such as those involving friction [16]. For comprehensive insight, the reader is encouraged to refer to Takens' original work [17]. By using a sphere-on-flat configuration, Hsia et al. [18] showed that the running-in period is a complex system, where a transition in the wear micromechanisms from ploughing to adhesion and mild wear of both contacts occurs, leading to a more stable friction response. In other words, the behaviour of friction is determined by the wear of the asperities and the effect of their presence on the pressure between the contact surfaces once most have worn.

Understanding the running-in period and its duration is an important topic that researchers are proposing different methods [19] beyond the current criteria based on the surface roughness, friction coefficient, and wear rate stabilization. Notably, the running-in period has a significant impact on the steady-state performance of a tribological system. Researchers have found that factors such as surface roughness and wear rate during the running-in period can directly affect the steady-state friction coefficient and wear behaviour. In fact, researchers have emphasized the need to further investigate the running-in process in terms of load, speed, and the duration needed to reach a steady state to determine the optimal operating conditions during running-in, which can result in the best steady-state performance. The abrasive wear is commonly subdivided into 2-body and 3-body abrasion or into low-stress and high-stress abrasion, according to Gates [20]. Recently, a study of the running-in period for austenitic steels was conducted under abrasive wear conditions [21], where a correlation between the stabilization of the hardness and the achievement of steady-state wear was found. In this work, it has been postulated that factors beyond hardness influence the running-in period for austenitic steels. For instance, the strain hardening of steel during the running-in period exhibits a strong correlation with the wear coefficient.

Running-in is a complex phenomenon that simultaneously involves elastic–plastic deformation in the asperities and microstructural and chemical changes in the mating surfaces. Because this phenomenon occurs in the industrial components that present slip between them, further study is needed to understand the nature of the running-in period. For this study, the changes occurring during the running-in period in austenitic steels varying the load and speed are correlated with the wear rate, wear mechanism, friction coefficient, hardening, and roughness. The selection of materials and operating conditions is essential for the control of the running-in period.

2 Material Characterization

2.1 Materials

The samples of Hadfield steel used in this work were extracted from the section of a hammer from the scrap shredder. The Hadfield steel section (material that comes from a casting process) of the hammer was extracted from a place that was not affected by the impact loads to which the hammer is subjected daily, as shown in Fig. 1. The extracted area of the Hadfield steel and the AISI 316L stainless steel were subjected to a solubilization treatment at 1100 °C for 2 h, using coal and metal shavings to avoid oxidation and decarburization of the surface, and then quenched in water. The selected material to serve as a counterbody in this work was an ASTM A36 steel (Sect. 2.4). The ASTM A36 disks were cut using a laser cutting process from an initially purchased ASTM A36 plate measuring 1 × 1 m. Several disks were produced with dimensions of 15 ± 0.01 mm in diameter and 5 ± 0.01 mm in thickness, achieving a R_a of 0.5 μm .

Pins of austenitic Hadfield steel and AISI 316L stainless steel were cut by electrodischarge machining (EDM) to the following dimensions: a 3 mm diameter and 33 mm length. Prior to the tribological tests (Sect. 2.4), the pins and disks were cleaned using ethanol and compressed air at a pressure of 100 Psi on their surfaces. The chemical composition is given

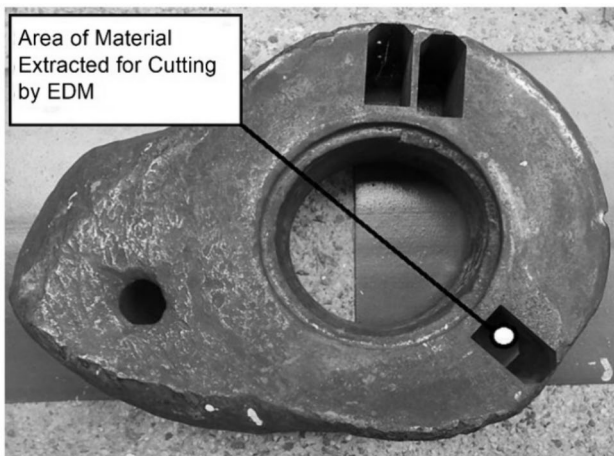


Fig. 1 Hadfield steel hammer from a scrap shredder, highlighting the area from which pins were extracted using electro-discharge machining (EDM)

in Table 1. These steels were selected based on two criteria. These criteria included the commercial availability, which facilitated the reproducibility of the present results by other research groups, and the well-known strain hardening capacity during deformation and wear [21, 22] due to the relatively low mechanical stability of the austenite, i.e. stacking fault energy [23–25]. This characteristic could facilitate the understanding of matrix strain hardening, wear behaviour, and running-in.

The Hadfield and AISI 316L steels possess austenitic microstructures (*f.c.c.* crystal structures) as depicted in Fig. 2.

2.2 Hardness

Micro-Vickers hardness (Buehler 1600 Series) testing was conducted with a load of 0.98 N for 15 s. To identify the change in hardness during the sliding test, the microhardness was measured every 30 m to the full length of 180 m. Hardness measurements were conducted using distinct pins for each test to ensure accuracy. After each stop, the pin was detached from the tribometer and subjected to mass and roughness measurements as required. Subsequently, the pin was placed in the microhardness tester where it was indented on the affected surface. A minimum of 10 hardness measurements were performed under each stop to ensure data reliability. The margin of error for these tests was determined with a 95% confidence interval. For subsequent tests, a new pin was employed to accurately ascertain changes in hardness.

2.3 Roughness Measurement

Surface roughness was determined before and after the sliding wear test for each steel using a profiler tester (Taylor Hobson model Talysurf CCI). A recorded area of 0.8 mm × 0.8 mm on the surface of each pin during each stop (Sect. 2.4) was utilized to ensure a more meaningful statistical significance regarding the roughness parameter that was determined. The operating parameters of the profilometer are given in Table 2. R_a represents the average roughness, calculated as the arithmetic mean of deviations from the roughness profile's central line. In this study, the selection of the R_a parameter over other areal parameters, such as S_a , S_q , S_{sk} , and S_{ku} , was driven by its universal acceptance and the facilitation of comparative analysis across diverse studies and industrial applications. The R_a parameter is recognized as a foundational metric for assessing surface roughness, providing a consistent basis for comparison, particularly pertinent when aligning results with

Table 1 Chemical compositions of the studied alloys and counterbody (wt%)

Alloy	C	Mn	Cr	Ni	Si	P	S	Mo	Cu
Hadfield	1.453	14.928	2.277	0.068	0.409	0.062	0.062	0.031	0.188
AISI 316L	0.032	2.002	18.030	10.010	1.012	0.045	0.031	2.010	–
ASTM A36	0.260	0.530	–	–	0.290	0.040	0.050	–	0.200

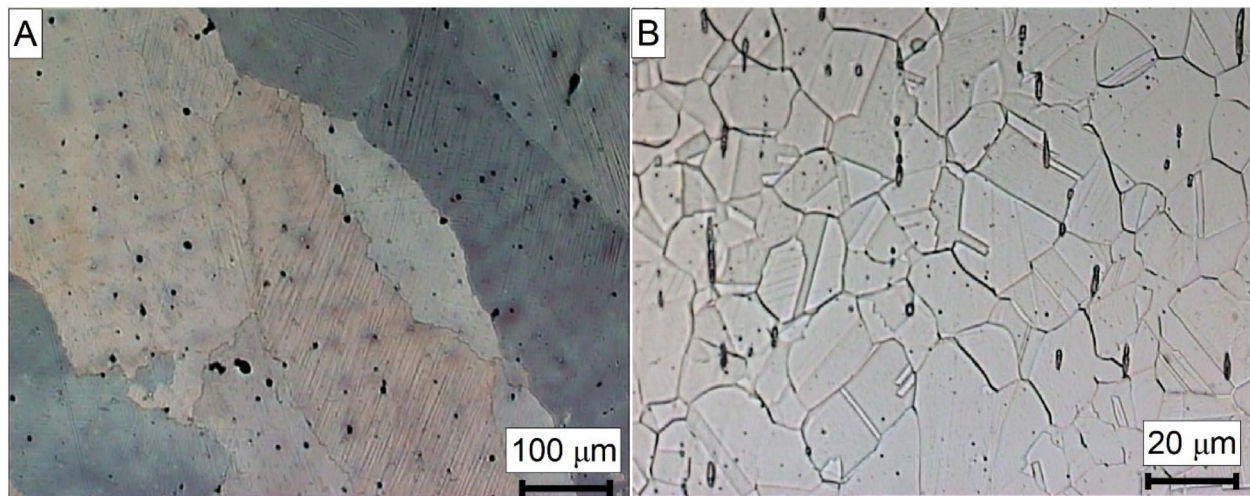


Fig. 2 Optical micrographs of the **a** Hadfield Steel and **b** AISI 316L steel

Table 2 Profilometer parameters (pin roughness measurement)

Parameters	Values
Roughness parameter	R_a
Velocity of displacement	0.25 mm/s
Measuring range	100 μm (resolution 0.1 μm)
Measured profile/filter	R-profile/Pc50
Spacing	1e-005 μm
Relation of non-measured points (NMP)	0.1611% (1689)
Height (measuring range)	31.97 μm (35.2 μm)
Resolution XY	0.82 μm
Visual field	0.842 mm
Lens	20 \times (WD 4.7 mm)
Cutting length (cut-off)	0.8 mm

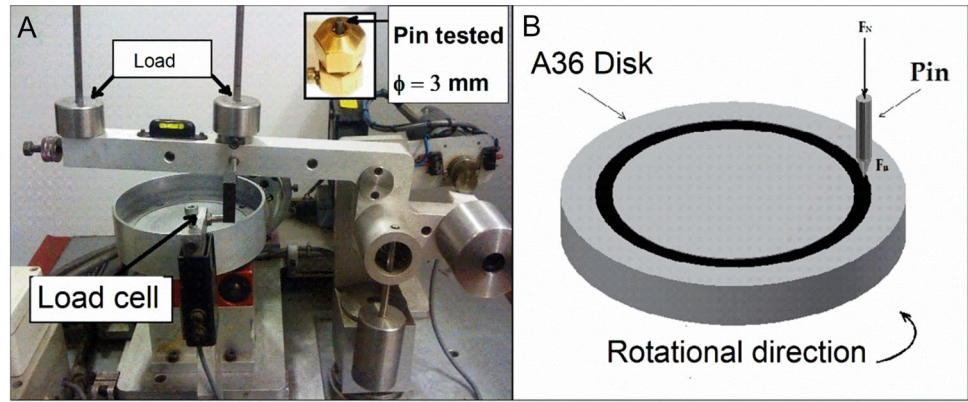
an extensive corpus of existing data that similarly employs R_a . This choice ensures that our findings are both comparable and compatible with the broader scientific and engineering communities, thereby enhancing the reproducibility and reliability of our work. The R-profile measures the optical intensity of the current beam, while the Pc50 filter manages light polarization, essential for analysing interference patterns with a spacing of 1e-005 μm . The non-measured points (NMP) ratio, at 0.1611%, reflects the proportion of points excluded from roughness calculations, indicating effective scanning coverage. The cut-off length, determined by Gaussian filters, distinguishes between roughness and waviness deviations.

2.4 Tribological Test

A Plint & Partners tribometer, model TE79 (Fig. 3), was used to conduct the sliding wear test. The selection of the test methodology was based on the guidelines presented in

the ASTM G99 standard [26]. However, ASTM A36 steel was selected as a counter body with a hardness of 137 ± 0.15 HV. This steel was selected to avoid quick strain hardening on the pin surfaces and to prolong the running-in period during the tests as much as possible to be able to record the roughness and hardness changes. The experimental procedure was conducted under two distinct normal loads and two sliding speeds: 6 N and 12 N, and 0.18 m/s and 0.70 m/s, respectively. The environmental conditions during the tests were maintained at a temperature of 30 °C and a relative humidity of 50%. Significant research related to the running-in in the context of sliding wear was conducted by Queener et al. [27]. This research established that total wear comprises two components: one linear (steady state) and the other transient (breaking-in or running-in). A model was proposed in this study and discussed in light of experimental results conducted by the same authors, as well as previous results from the literature. It was concluded that the transient contribution (running-in) to total wear is proportional to the initial surface roughness. Based on that research, in the present study, the initial surface values for all evaluated conditions were set to be the same, as it will be described shortly, in order to mitigate the influence of the initial surface on the running-in period in terms of wear coefficient, friction, or hardness. Prior to the tribological test, a settlement process was implemented. This process utilized a normal load of 1 N over a travel distance of 5 m, employing a 1200 grit SiC abrasive paper. The objective was to homogenize the surfaces of the interacting materials, thereby mitigating any influence of each coupon's initial roughness on the development of the running-in phase. Following this process, the Hadfield and AISI 316L pins achieved a R_a roughness of 0.0873 μm and 0.1016 μm , respectively, while the disks achieved a roughness of 0.5 μm . Henceforth, these surface

Fig. 3 Test device used in pin (flat-ended)-on-disk configuration



finishing conditions will be considered as the initial roughness conditions.

To monitor the alterations during the initial phase of the running-in, preliminary tests were implemented. It was established that to attain adequate statistical validity, six interruptions should be incorporated during each test condition. This implies that interruptions were scheduled every 30 m until a total distance of 180 m was covered. Furthermore, to ensure the validity of the results, three repetitions of the tribological tests were conducted, strictly following the methodology described in [21]. In particular, each tribological test and characterization (including wear coefficient, hardness, roughness, etc.) was performed at least 3 times at each predefined stop. As a result, the error bars depicted in each graph correspond to this deviation. Additionally, to ensure the precision of the test, the equipment was programmed to halt at each predetermined stop, conduct the necessary mass, hardness (Sect. 2.2), and roughness measurements, and then resume the tribological test until the next stop.

The specific wear rate, which is expressed as the volume removed per unit load per unit sliding distance (k), was determined by employing Eq. (1) [21]:

$$k (\text{mm}^3/\text{Nm}) = \frac{\Delta m}{\rho L F_N}, \quad (1)$$

where Δm is the change in weight before and after wear for each type of steel (five measurements of weight change were conducted, and the mean value of these measurements was used in this analysis), ρ is the density (the density of Hadfield steel is 7.8 g/cm^3 , while the density of AISI 316 steel is 7.9 g/cm^3), F_N is the normal load, and L is the sliding distance. For clarity, it is important to mention that we are utilizing accumulated k values. In other words, Eq. 1 is calculated considering the total mass loss and the total distance travelled up to each stop. The wear coefficient K , as highlighted by Stachowiak [28], has two commonly used meanings in the literature which could be puzzling. One is under

the Archard postulate, which introduces the proportionality constant (dimensionless [29]) between the real contact area, sliding distance, and the wear volume, i.e. $V = K A_r l = K l W / H$, where: V is the wear volume [m^3]; K is the proportionality constant; A_r is the real area of the contact [m^2]; W is the load [N]; H is the Vickers hardness of the softer surface [Pa]; l is the sliding distance [m]. The other meaning of k is the specific wear rate, which is defined as $k = V / W \times L$, where: k is the specific wear rate (sometimes called the ‘wear factor’) [m^3/Nm]; V is the wear volume [m^3] or the same as $\Delta m / \rho$; W is the normal load [N]; L is the sliding distance [m]. Note that in this latest definition, k does not include hardness. Since in this work, the hardness evolved significantly during the running-in period, and a single bulk initial hardness (static hardness) of the steel would have led to difficulties in interpreting the data, the latter meaning of the wear coefficient was considered in this work.

3 Results and Discussion

3.1 Wear Results

The wear coefficient (k) vs. travelled distance was plotted for all evaluated conditions. The dashed lines in the graphs indicate that the specimens have reached a constant wear rate, allowing for the differentiation of the running-in and steady-stage periods. However, the authors wish to emphasize that determining the steady state or the conclusion of the running-in period based solely on the k values is somewhat arbitrary. The choice of this point was made considering the minimal difference in the mean value before and after the stop being analysed. It is important to consider other factors when establishing the running-in period, which will be discussed in the following sections.

3.1.1 Hadfield Steel

Figure 4 shows the wear coefficients (k) as a function of the sliding distance (m) of Hadfield steel tested at sliding speeds of 0.18 and 0.70 (m/s) for normal loads of 6 N and 12 N. Two general trends from this graph can be drawn. First, as the normal load increases from 6 to 12 N for all sliding speeds, the k value increases by one order of magnitude, which is expected with the well-known role of increasing the normal load in wear. Second, increasing the sliding speed (m/s) from 0.18 to 0.70 increased the k value regardless of the normal load used. When analysing the results at a more detailed level, it can be seen that the sliding speed has an effect on the running-in period (from the k point of view). For instance, Fig. 4a shows that the running-in period for 0.18 m/s is approximately 120 m, while for 0.70 m/s, it is approximately 150 m. On the other hand, as the normal load increases from 6 to 12 N, Fig. 4b illustrates that the running-in period for the condition tested at 12 N with a speed of 0.18 m/s is longer than the condition tested at 6 N with the same speed, as shown in Fig. 4a.

Notably, the k values stabilize at approximately 120 m and 150 m for the conditions tested at 6 N and 12 N at a sliding speed of 0.18 m/s, respectively. This finding coincides well with the stabilization of hardness, as will be shown later (Fig. 14a, b).

3.1.2 AISI 316L Steel

Figure 5 shows the wear coefficients (k) as a function of the sliding distance (m) of the AISI 316L steel tested at sliding speeds of 0.18 and 0.70 (m/s) under normal loads of 6 N and 12 N. Similarly, as in the Hadfield steel (Sect. 3.1.1),

increasing the sliding speed from 0.18 and 0.70 m/s increases the k value regardless of the normal load used. However, a noticeable difference from what occurred in the Hadfield steel (Sect. 3.1.1) is that as the normal load increases from 6 to 12 N, the k value decreases for the condition tested at a 0.70 m/s sliding speed.

In addition, it is worth mentioning that the k value stabilizes at approximately 150 m and 60 m for the conditions tested at 6 N and 12 N at a sliding speed of 0.18 m/s, respectively. This finding is in agreement with the stabilization of hardness, as will be shown later (Fig. 15a, b).

3.1.3 Instantaneous Wear Rate Discussion

The cumulative k values discussed in the previous section showed that the values stabilized after a certain sliding distance for both Hadfield and AISI 316L stainless steel, irrespective of the normal load or sliding speed used. However, the running-in period could also be analysed from another perspective that is, using instantaneous values. The following analysis is based on the work of Peter Blau [6], where it is concluded that the wear rates (i.e. the slope of the curve connecting the beginning of the test with its endpoint) can vary significantly depending on the interval chosen to define the test duration. In Fig. 6, the volume loss (mm^3) versus sliding distance (m) for both Hadfield and AISI 316L stainless steel is shown.

In Fig. 6a, different red lines are drawn to assess the slope and determine if the running-in period has finished and the steady state has begun for the condition of 6 N and 0.70 m/s in the Hadfield steel. For example, line OB represents a high wear rate condition typically associated with the running-in, where its slope (S_{OB}) is 1.21, equivalent to the instantaneous

Fig. 4 Wear coefficient (k) as a function of the sliding distance (m) of Hadfield steel at sliding speeds of 0.18 and 0.70 m/s under normal loading: **a** 6 N and **b** 12 N

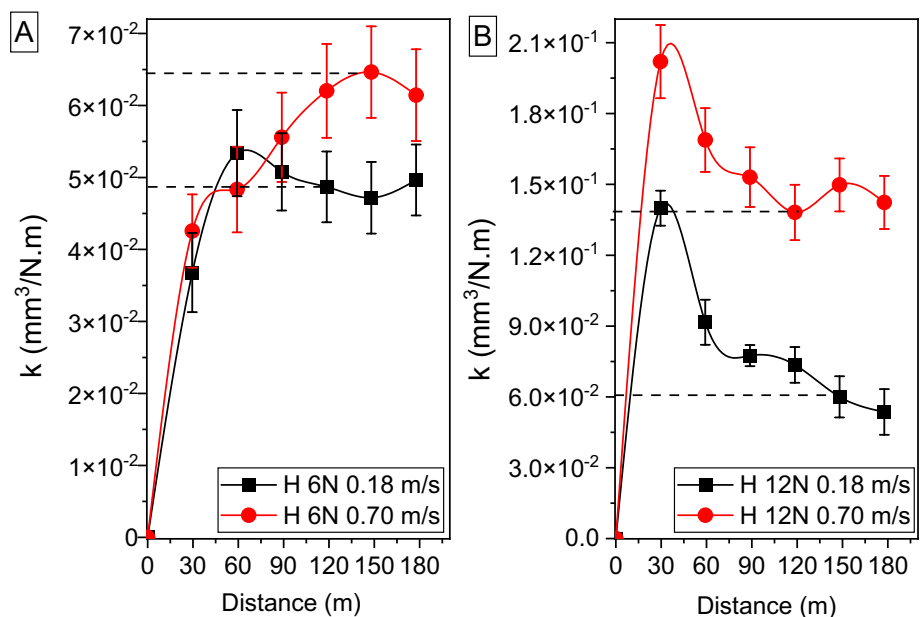


Fig. 5 Wear coefficient (k) as a function of the sliding distance (m) and of the AISI 316L steel at sliding speeds of 0.18 and 0.70 m/s under normal loads: **a** 6 N and **b** 12 N

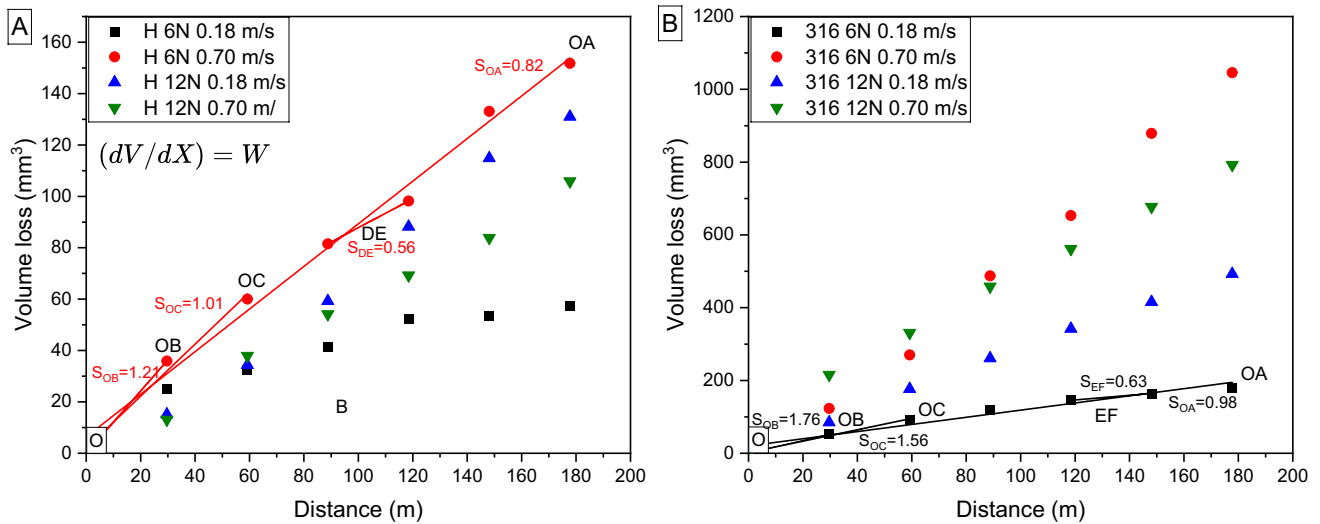
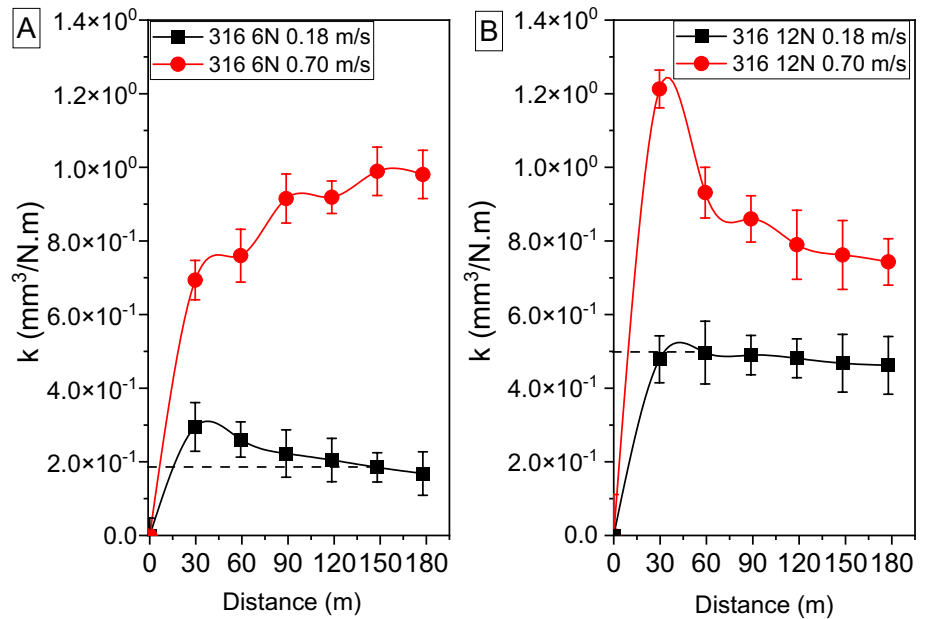


Fig. 6 Volume loss (mm^3) versus sliding distance (m) of the **a** Hadfield steel (H) and **b** AISI 316L stainless steel, where S is the slope determined from the final point to the origin, and it is equivalent to W , the instantaneous wear rate

wear rate (W). Similar comments apply to line OC, where the slope (S_{OC} is 1.01). The line DE, the slope (S_{DE}) is 0.56, suggesting that the running-in period has probably finished. Finally, line OA represents the case where the test ends only after a transition to a high rate of wear-out. The slope of that line is clearly affected by the wear-out phase. At the distance of 90 m, the steady-state period determined from the instantaneous wear rate of the condition coincides with the hardness stabilization of this material at 90 m, as will be discussed in Sect. 3.4.1. Following a similar analysis for the AISI 316L stainless steel tested at 6 N and 0.18 m/s, as shown in Fig. 6b it is clear that the slope of line EF

drastically decreases compared to the slope values in the initial meters of the sliding distance. When calculating the slope of the subsequent straight line from point F to point A, the slope value was 0.59, which confirms that the stabilization of the instantaneous wear rate was achieved. Lastly, but not least, it is of utmost importance to mention that the end of the running-in period and the start of the steady state in a tribosystem are not necessarily defined solely by the stabilization of the wear rate. Other key factors such as the steady state of hardness, surface roughness, and friction coefficient could also mark the end of the running-in period, as this work demonstrates.

3.2 Friction Coefficient

Figure 7 displays the average friction coefficient (μ), determined from three friction curves, plotted against distance (m) for both AISI 316L steel and Hadfield steel under two different sets of conditions: 6 N and 0.18 m/s and 12 N and 0.7 m/s. The results show that the lowest sliding speed leads to the lowest friction coefficients. A strong correlation can be observed between μ and surface roughness (Fig. 13). For example, the μ for Hadfield steel tested at 6 N and 0.18 m/s is significantly lower than that tested at 12 N and 0.70 m/s. This trend is also reflected in the average surface roughness (R_a) values, as shown in Fig. 11, where the R_a for Hadfield steel tested at 6 N and 0.18 m/s is much lower than that tested at 12 N and 0.70 m/s. This correlation is evident for AISI 316L SS, where the μ for AISI 316L SS tested at 6 N and 0.18 m/s is much lower than that tested at 12 N and 0.70 m/s. The R_a for AISI 316L SS tested at 6 N and 0.18 m/s is much lower than that tested at 12 N and 0.70 m/s.

The different steady-state μ values acquired from Fig. 7 for both AISI 316L steel and Hadfield steel under two different sets of conditions, 6 N and 0.18 m/s and 12 N and 0.7 m/s, are shown in Fig. 8. While it is generally expected that the wear coefficient and friction coefficient are load- and speed-independent, there are numerous studies in the literature that have reported a dependence of these coefficients on load and speed under certain conditions. For instance, studies by Yokohata et al. [30], Xu et al. [31], and Zambrano et al. [32] have shown that for certain materials and under specific operating conditions, the wear and friction coefficients can be load and speed-dependent. In this study, a

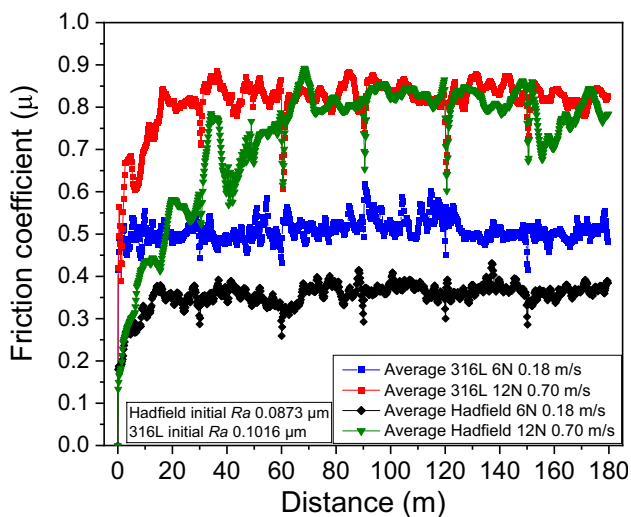


Fig. 7 Average friction coefficient (μ) (determined from three friction curves) against distance (m) for the AISI 316L steel and Hadfield steel at 6 N with the lowest sliding speed and 12 N with the highest sliding speed. The initial roughness condition (R_a) is shown

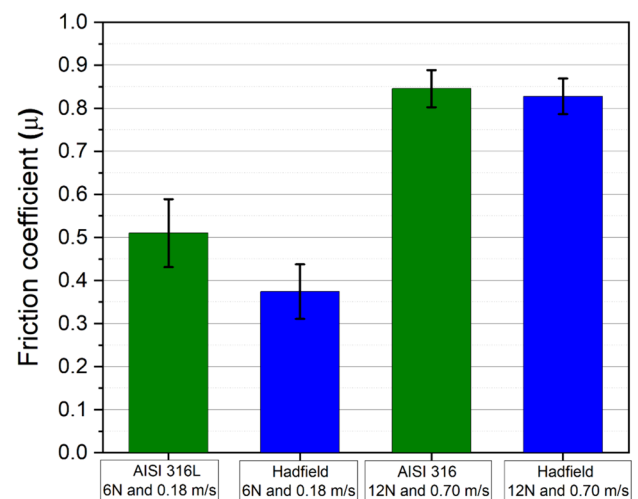


Fig. 8 Friction coefficient (μ) values of the AISI 316L steel and Hadfield steel at 6 N with the lowest sliding speed (0.18 m/s) and 12 N with the highest sliding speed (0.70 m/s)

similar trend was observed for austenitic steels in a pin-on-disk configuration. This could be attributed to several factors such as the operating conditions, the specific tribological system used in these experiments, and the material properties such as strain hardenability and plastic deformation mechanisms that may significantly alter the contact mechanics between asperities.

The friction coefficient results shown in Fig. 8 agree with the wear surfaces (Sect. 3.1). Under low loads and speeds, the AISI 316L steel has a higher μ than the Hadfield steel, and the surface of the AISI 316L steel shows more severe plastic deformation, microcutting, and particle adherence.

3.3 Roughness

Figure 9 shows the topographic profile of the pins of Hadfield steel under normal loads of 6 N and 12 N at sliding speeds of 0.18 m/s and 0.70 m/s after the test (180 m). Figure 10 shows the topographic profiles of the pins of AISI 316L stainless steel under normal loads of 6 N and 12 N at sliding speeds of 0.18 m/s and 0.70 m/s after the test (180 m). Figure 11 shows the variation in the average roughness (R_a) with respect to the sliding distance. For AISI 316L steel (Fig. 11a), the sliding speed is the main variable that affects the average roughness of worn surfaces, regardless of the normal load. The sliding speed of 0.70 m/s has a greater effect on increasing the sizes of the peaks than 0.18 m/s. The effect of sliding speed is particularly noticeable under a normal load of 6 N, as shown in (Fig. 11a). The peak heights change significantly, as observed on comparing Fig. 10a, b. In addition, it is reasonable to infer that R_a has a good relationship with the k value. There is a higher k value for AISI 316L SS at 6 N and 0.70 m/s than at 12 N and

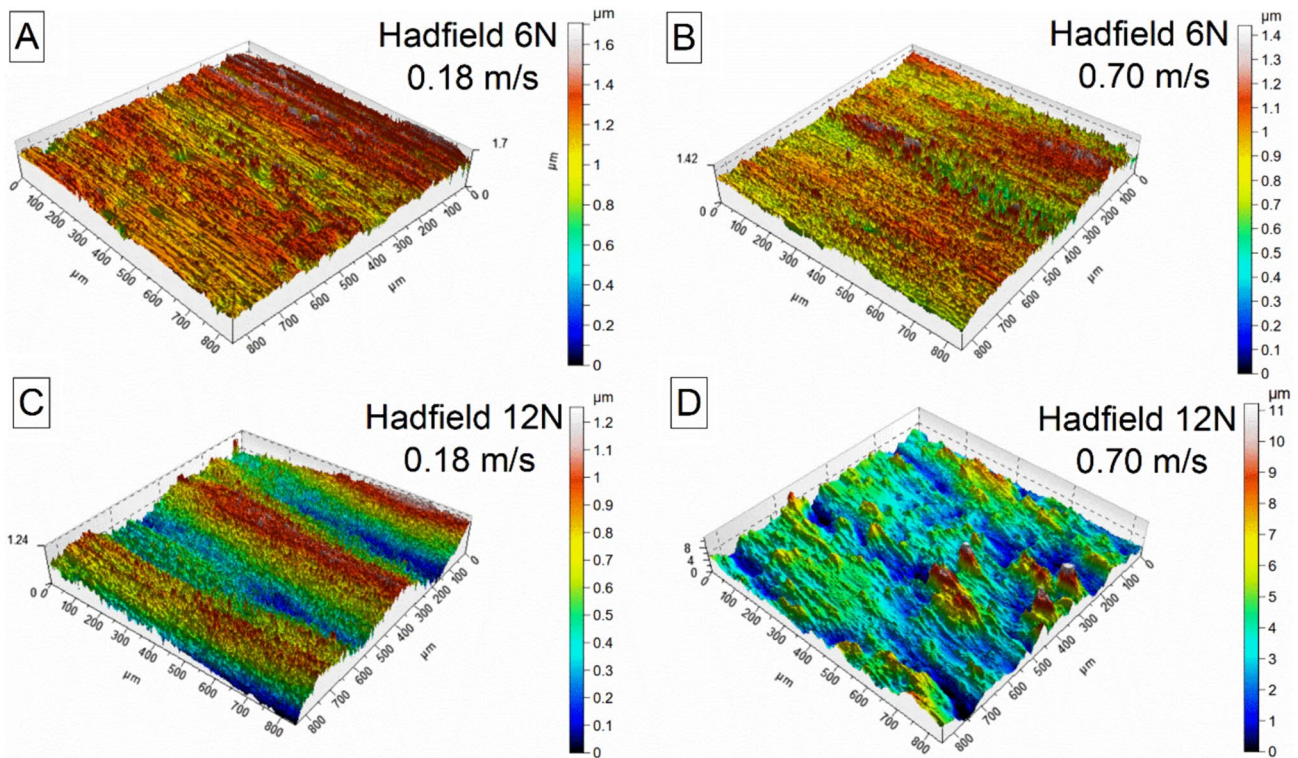


Fig. 9 Topographic profiles of the pins of Hadfield steel at the end of the test (180 m) under a normal load of 6 N at sliding speeds of **a** 0.18 m/s and **b** 0.70 m/s and under a normal load of 12 N at sliding

speeds of **c** 0.18 m/s and **d** 0.70 m/s. The initial roughness condition (R_a) for the Hadfield steel is 0.0873 μm

0.70 m/s, corresponding to high and low R_a values, respectively. Conversely, it is relevant to mention that for the tests carried out with Hadfield steel (Fig. 11b), the sliding speed is the factor with the greatest influence on the increases in average roughness and worn topography. The conditions that have the greatest influence on the variability of the average R_a in tests carried out with Hadfield steel are the highest load (12 N) and the highest sliding speed (0.70 m/s). This finding is in agreement with the greatest friction coefficient observed in Fig. 7, 8 and with the high R_a values measured in Fig. 9d. Notably, by analysing the wear coefficient (Fig. 5) and the roughness (Fig. 11a) of AISI 316L steel, it appears that a relatively high load for the AISI 316L steel decreases the running-in distance (perhaps due to its low hardness, indicating the rapid deformation of asperities). A faster stabilization of roughness is observed at high loads (short peak-to-valley distance), which is consistent with the results of Sjöberg et al. [33]. In a similar line of analysis, by reviewing the wear coefficient of the Hadfield steel (Fig. 4), it is evident that the condition with the highest k (Hadfield 12 N and 0.7 m/s) has the highest roughness at the end of the running-in period (125 m); it seems that this phenomenon is the case with the AISI 316L SS. These observations are consistent with the discussion of Akbarzadeh et al. [34].

Figure 12 shows the final roughness values (after 180 m) for both steels. The 316L steel exhibits greater roughness and greater surface damage than Hadfield steel, as can be observed by SEM (and respectively).

Figure 13 presents the comparative analysis of the average friction coefficient (μ) against roughness R_a (μm) for AISI 316L steel and Hadfield steel under two distinct conditions: a load of 6 N at the minimum sliding speed, and a load of 12 N at the maximum sliding speed. A discernible correlation is evident within each steel type between the steady-state friction coefficient and the roughness at 180 m. Furthermore, an increase in either the normal load or the sliding speed results in a corresponding increase in both the friction coefficient and roughness. This observation underscores the interdependent relationship between these variables.

3.4 Hardness

3.4.1 Hadfield Steel

Figure 14 shows the hardness profile of Hadfield steel using sliding speeds of 0.18 m/s and 0.70 m/s under normal loads of 6 N and 12 N, respectively. The first point to note is that increasing the normal load from 6 to 12 N

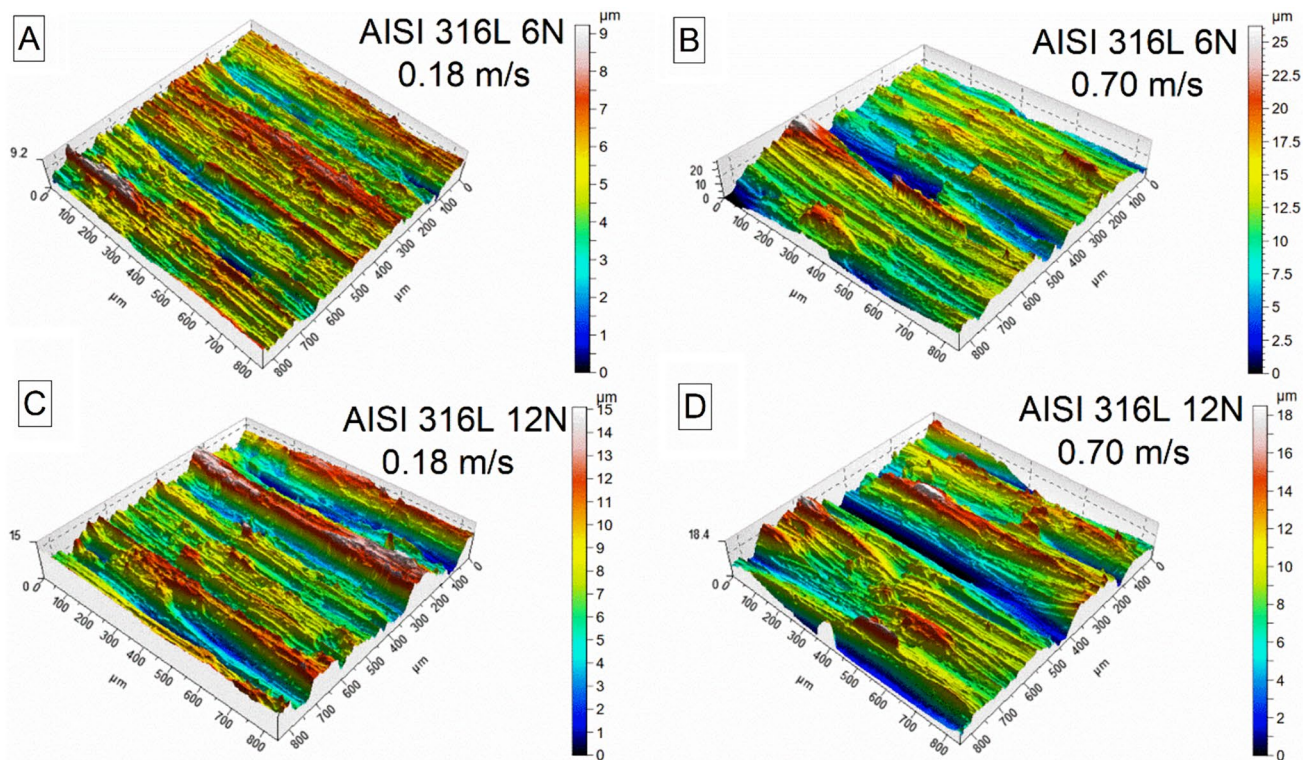
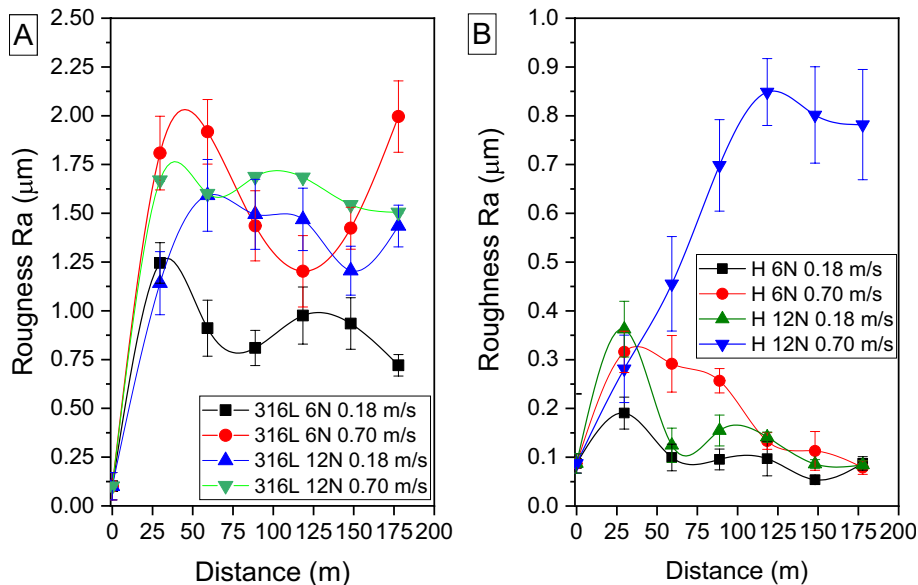


Fig. 10 Topographic profiles of the pins of AISI 316L steel after the test (180 m) under a normal load of 6 N at sliding speeds of **a** 0.18 m/s and **b** 0.70 m/s and under a normal load of 12 N at sliding

speeds of **c** 0.18 m/s and **d** 0.70 m/s. The initial roughness condition (R_a) for the AISI 316L steel is 0.1016 μm

Fig. 11 Change in roughness (R_a) during the sliding wear test as a function of normal load (N) and sliding speed (m/s) for **a** AISI 316L stainless steel and **b** Hadfield steel (*H*)



drastically increases the hardness during the running-in period. Nonetheless, the effect of the normal load in delimiting the running-in period is more obscure. At a sliding speed of 0.70 m/s, increasing the normal load from 6 to 12 N has a negligible effect on the running-in period and

the maximum hardness achieved during the steady state. In contrast, for the conditions tested at a sliding speed of 0.18 m/s, the effect of the normal load can be appreciated; that is, as the normal load increases, the maximum

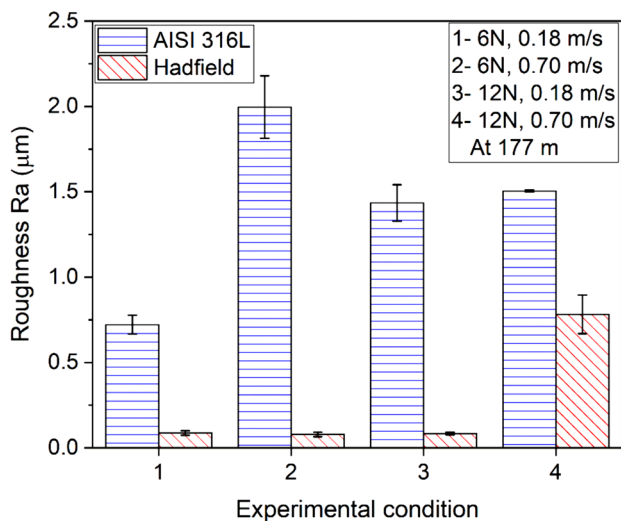


Fig. 12 Final roughness (R_a) of AISI 316L steel and Hadfield steel as a function of normal load (N) and sliding speed (m/s). The initial roughness condition (R_a) for the Hadfield and AISI 316L steels are 0.0873 μm and 0.1016 μm , respectively

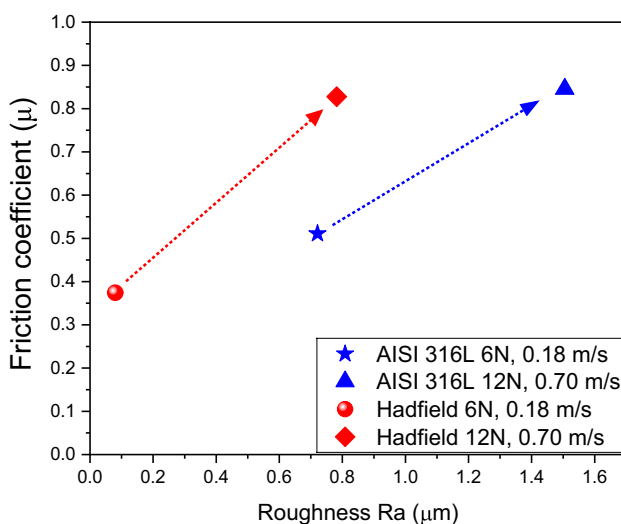


Fig. 13 Average friction coefficient (μ) against roughness R_a (μm) for the AISI 316L steel and Hadfield steel at 6 N with the lowest sliding speed and 12 N with the highest sliding speed

hardness achieved increases, and the running-in period seems to be longer under a load of 12 N.

The hardness of the Hadfield steel stabilizes at 120 m under a load of 6 N and a speed of 0.18 m/s, while it stabilizes at 90 m under a load of 6 N and a speed of 0.70 m/s. At 12 N, the Hadfield steel stabilizes at approximately 150 m at 0.18 m/s, while it stabilizes at 90 m at a speed of 0.70 m/s. Based on these results, it seems that the sliding speed has a relevant impact on the strain hardenability, a topic that is discussed in Sect. 3.4.3.

3.4.2 AISI 316L Steel

Figure 15 shows the hardness profile of the AISI 316L steel using sliding speeds of 0.18 m/s and 0.70 m/s under normal loads of 6 N and 12 N, respectively. Similarly, as in the case of the Hadfield steel (Sect. 3.4.1), as the normal load increases from 6 to 12 N, the hardness increases drastically during the running-in period. For instance, for 316L steel tested under the conditions of 6 N and 0.70 m/s at 30 m, the hardness increases from ~ 250 to ~ 325 HV. However, for 316L steel tested under the conditions of 12 N and 0.70 m/s at 30 m, the hardness increases from ~ 250 to ~ 425 HV. Thus, the normal load plays an important role in the strain hardening rate of austenite during the running-in period. Another important effect is the sliding speed. At either 6 N or 12 N, when the sliding speed increases, the slower sliding speed leads to the quicker strain hardening of the austenite.

The hardness of the AISI 316L stainless steel stabilizes at 90 m under the conditions of 6 N and 0.18 m/s. Later, steel stabilizes to 150 m due to the strain hardening layer detachment. Similar oscillatory behaviour is observed for the condition tested at 0.70 m/s. At 12 N, the AISI 316L SS stabilizes at approximately 60 m at 0.18 m/s, while it stabilizes at 150 m at 0.70 m/s. Based on these results, it seems that the sliding speed has a relevant impact on the strain hardenability, especially during the running-in period, which is discussed in Sect. 3.4.3.

3.4.3 Hardness Changes During the Running-in Observed for the Hadfield Steel and AISI 316L Stainless Steel

In addition to the running-in period in both austenitic steels, it is interesting to observe that the maximum hardness reached during the studied conditions in the Hadfield steel is much higher than that reached by the AISI 316L steel. Here, it is convenient to discuss the concept of the stacking fault energy (SFE) [35], which determines the stability of austenite and its susceptibility to deformation-induced transformations and strain hardening capacities that can increase the plasticity during deformation. The SFE affects the formation of microstructural features, such as ϵ -martensite, α' -martensite, mechanical twins, and slip dislocations. Different authors have reported SFE value ranges, where these deformation mechanisms are predominant. Plastic deformation mechanisms can generally be classified based on the SFE value: transformation-induced plasticity (TRIP) occurs when the SFE is below 20 mJ/m^2 , twin-induced plasticity (TWIP) occurs when the SFE is between 20 mJ/m^2 and 40 mJ/m^2 , and microband-induced plasticity (MBIP) occurs when the SFE is above 40 mJ/m^2 [23, 24, 35, 36]. The SFE of the Hadfield steel is estimated to be approximately 23 mJ/m^2 at 298.15 K [37], which is lower than the estimated 40–64 mJ/m^2 for AISI

Fig. 14 Hardness profile of Hadfield steel at sliding speeds of 0.18 m/s and 0.70 m/s under normal loads of **a**6 N and **b**12 N

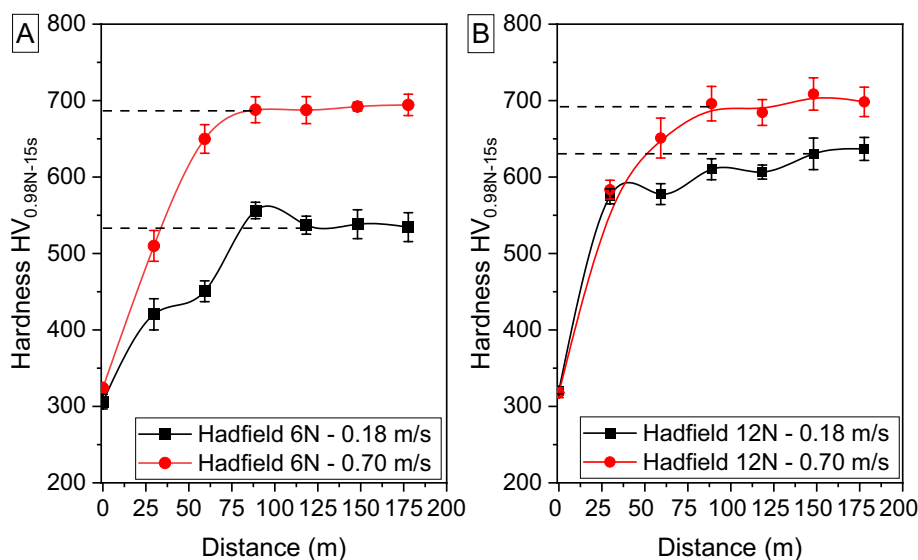
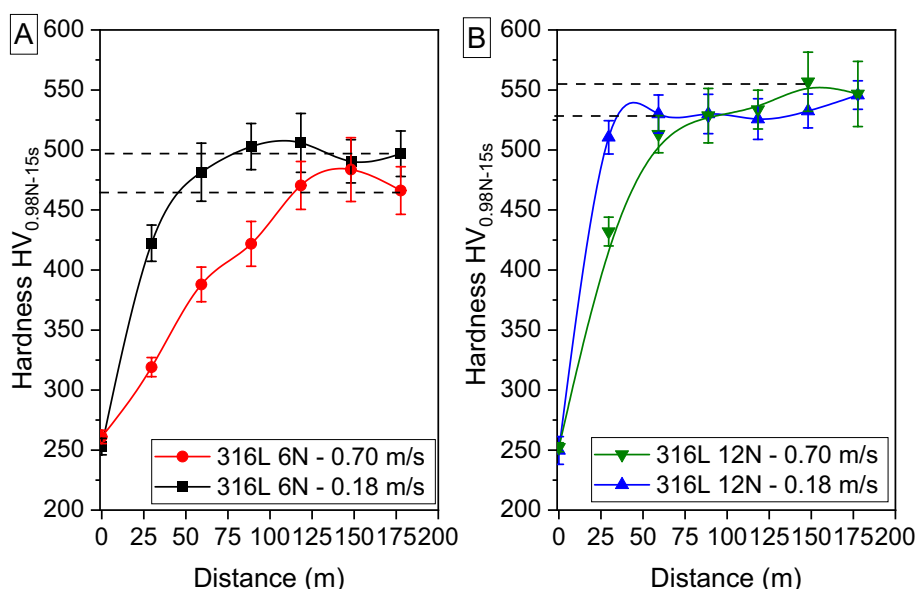


Fig. 15 Hardness profile of AISI 316L steel at sliding speeds of 0.18 m/s and 0.70 m/s under normal loads of **a**6 N and **b**12 N



316 stainless steel [22, 38]. Therefore, it is reasonable to expect that the operation of twinning can lead to higher hardness increases in the Hadfield steel under the conditions imposed in this study. However, the formation of microbands and some twinning can occur in the AISI 316L stainless steel, which can be less effective as a dislocation barrier than predominant twinning. Therefore, it is reasonable to expect that the AISI 316L steel can reduce the strain hardening rate capacity compared with that of Hadfield steel. These results align very well with those recently presented in [39], where the strain hardening percentage after abrasion wear of austenitic alloys decreases from 66 to 53% as the SFE of the austenite increases from 30.96 to 52.36 mJ/m². Therefore, it is reasonable to expect

that AISI 316L steel can have a lower strain hardening rate capacity than Hadfield steel.

It is important to note that the strain hardening behaviour of austenitic steels during wear conditions is a complex phenomenon that is influenced by a multitude of factors; the specific chemical composition of the steel plays a significant role. High-Mn austenitic steels, for instance, have been shown to exhibit excellent mechanical properties and adjustable strain hardening behaviour due to different deformation mechanisms [35, 40]. The SFE, which is influenced by the chemical composition and temperature, is a key factor in determining these deformation mechanisms. Another point to consider is that the tribological system employed in the experiments can have an impact on the strain hardening

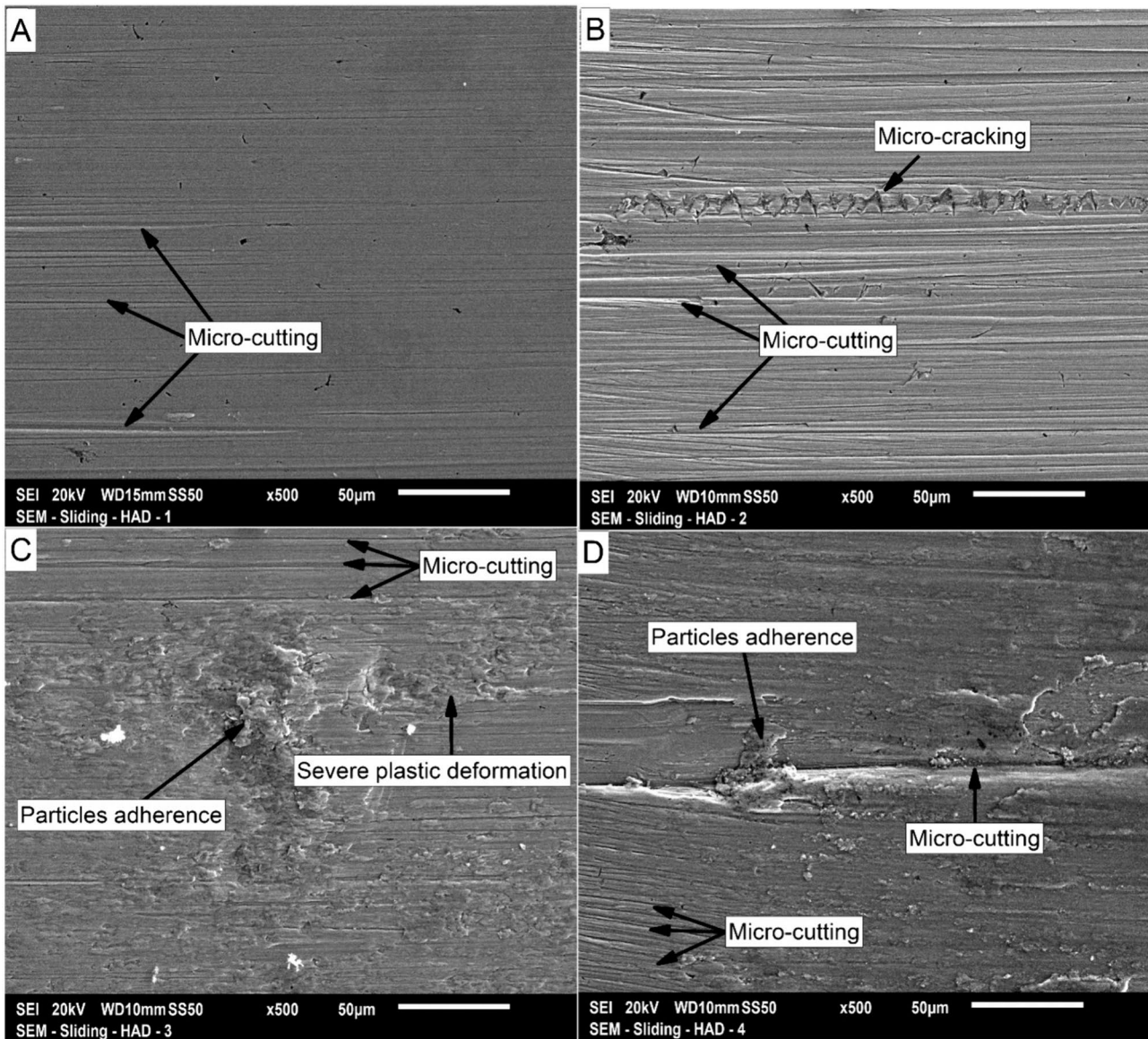


Fig. 16 Wear surfaces of Hadfield steel under a normal load of 6 N at a sliding speed of 0.18 m/s for different distances: **a** 30 m, **b** 60 m, **c** 90 m, and **d** 180 m

behaviour. For example, it was observed that the resistance to wear and corrosion of 316L austenitic stainless steel enhanced following strain hardening [41]. Concurrently, the average friction coefficients of the stainless steel showed a reduction as strain hardening increased. In summary, the strain hardening phenomena observed in austenitic steels under wear conditions is a complex interplay of various factors. These include the chemical composition of the material, the conditions under which the material operates, the specific tribological system in use, and the inherent properties of the material itself. To fully elucidate these intricate relationships and their subsequent effects on the wear

performance of austenitic steels, additional scientific investigation is warranted.

3.5 Wear Surfaces

3.5.1 Hadfield Steel

Figure 16 shows the wear surfaces of the Hadfield steel at different distances—30 m, 60 m, 90 m, and 180 m—under the conditions tested at 6 N and 0.18 m/s. At 30 m, the wear surface shows characteristics of fine grooves caused by microcutting. At 60 m, in addition to microcutting, some presumable microcracking and/or material detachment can

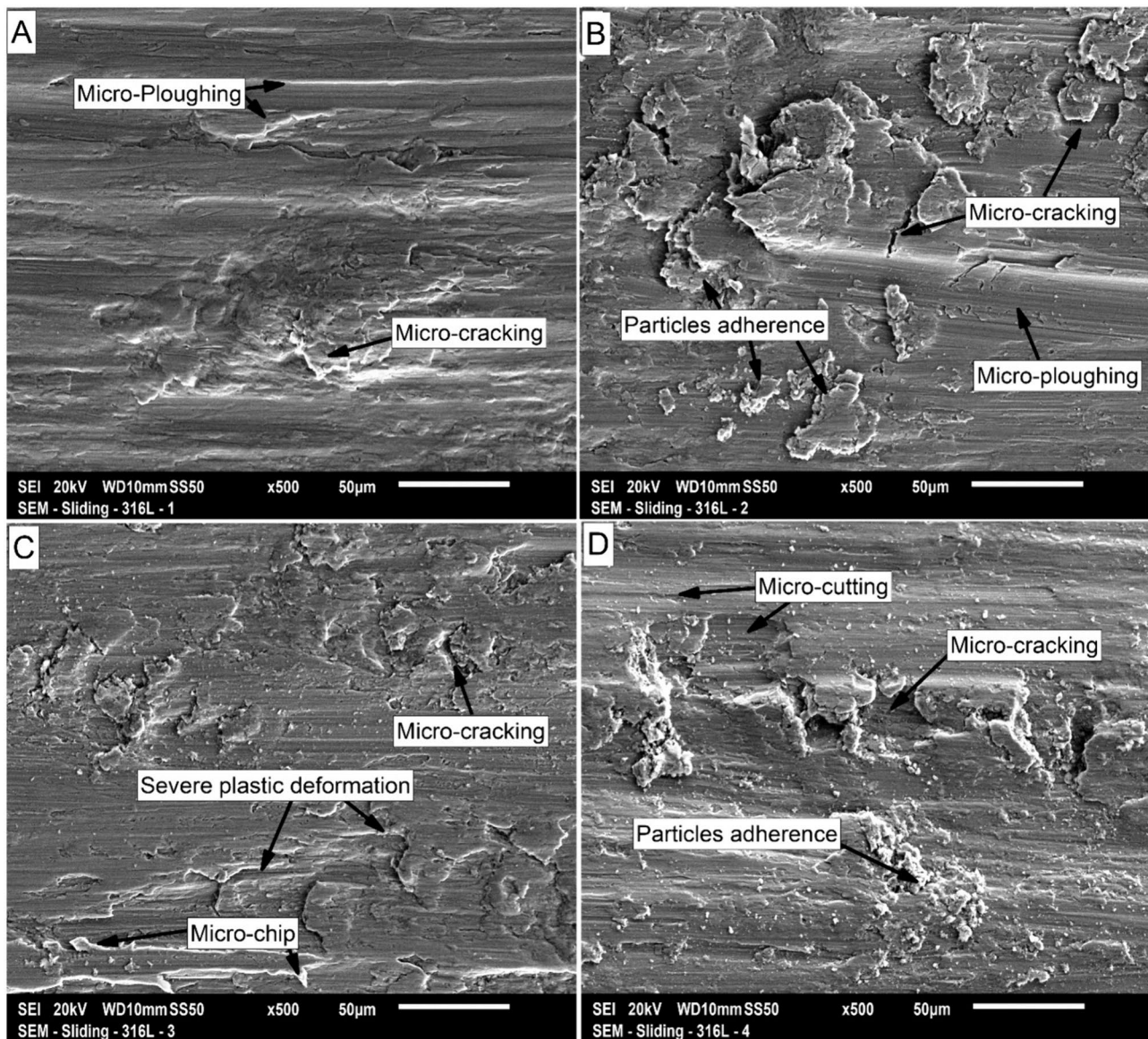


Fig. 17 Wear surfaces of AISI 316L steel under a normal load of 6 N at a sliding speed of 0.18 m/s for different distances **a** 30 m, **b** 60 m, **c** 90 m, and **d** 180 m

be observed. At 90 m, noticeable plastic deformation is observed, which is most likely due to the intimate contact with the counterbody after the asperities are settled; this settlement and some particle adherence occur during micro-cutting. At 180 m, similar features as in the case before can be observed, and the main difference is a less pronounced operation of plastic deformation. It is worth noting that there is a reasonable agreement among the k value during running-in and stabilization periods (Fig. 4a), the strain hardening caused by plastic deformation observed in Fig. 14a, and the wear micromechanisms observed.

Under this condition, the Hadfield steel seems to show a roughness stabilization of approximately 60 m (Fig. 11b), and not much fluctuation from the roughness viewpoint can be observed. This rapid stabilization matches the relatively uniform and homogenous changes in the micromechanism of the wear surface observed in Fig. 16.

3.5.2 AISI 316L Steel

Figure 17 shows the wear surfaces of the AISI 316L SS at different distances of 30 m, 60 m, 90 m, and 180 m under

the conditions of 6 N and 0.18 m/s. It is interesting that at 30 m, the wear surface only shows features of microcracking and microplothing. However, at distances of 60 m, 90 m, and 180 m, the identified wear micromechanisms, such as microcracking, microplothing, and adherence of particles from the counterbody, are quite similar.

It is worthwhile to mention that under this condition, the AISI 316L SS does not show roughness stabilization based on Fig. 11. However, there are wide fluctuations in amplitude due to the detachment or peeling off the material, matching the observations found through SEM in Fig. 17.

4 Conclusions

In this research, the running-in periods of austenitic steels in sliding wear are analysed using a pin-on-disk configuration. The following conclusions can be drawn:

The point at which the specific wear rate and hardness stabilize was observed to coincide with the end of the specified running-in period.

The lowest sliding speed leads to the lowest friction coefficient, roughness, and wear coefficient values.

During the running-in period, the wear surfaces of both Hadfield steel and AISI 316 stainless steel exhibit a strong correlation with changes in roughness.

The stability of the austenite, which is related to the stacking fault energy, appears to play a significant role during the running-in period of hardness in austenitic steels. This, in turn, is strongly associated with the running-in period observed during wear.

The k value for Hadfield steel increases by a factor of approximately 3 when the normal load is doubled from 6 to 12 N. However, for the AISI 316L steel, the same increase in the normal load only causes a slight increase in the k value within the same order of magnitude. Nevertheless, the k value is always lower for the Hadfield steel than for the AISI 316L steel.

Acknowledgements The authors acknowledge the support of Laboratório de Fenômenos de Superfície (LFS) at the Universidad de Sao Paulo (Brazil).

Author contributions O.A. Zambrano: Analysis of data, writing original draft, and final revision of the paper. B. Iglesias-Guerrero: Conducted the experiments, analysis of data, and final revision of the paper. S.A. Rodríguez: Concept and design of experiments, analysis of data, and final revision of the paper. J.J. Coronado: Concept and design of experiments, analysis of data, and final revision of the paper.

Funding Open access funding provided by National Research Council Canada library. This research received no specific grant from any funding agency in the public, commercial, or not-for-profit sectors.

Data availability Data will be made available on request.

Declarations

Competing interests The authors declare no competing interests.

Open Access This article is licensed under a Creative Commons Attribution 4.0 International License, which permits use, sharing, adaptation, distribution and reproduction in any medium or format, as long as you give appropriate credit to the original author(s) and the source, provide a link to the Creative Commons licence, and indicate if changes were made. The images or other third party material in this article are included in the article's Creative Commons licence, unless indicated otherwise in a credit line to the material. If material is not included in the article's Creative Commons licence and your intended use is not permitted by statutory regulation or exceeds the permitted use, you will need to obtain permission directly from the copyright holder. To view a copy of this licence, visit <http://creativecommons.org/licenses/by/4.0/>.

References

- Blau, P.J.: Running-in: art or engineering? *J. Mater. Eng.* **13**(1), 47–53 (1991)
- Zambrano, O.A., Coronado, J.J., Rodríguez, S.A.: Tempering temperature effect on sliding wear at high temperatures in mottled cast iron. *Tribol. Lett.* **57**(2), 19 (2015)
- Khonsari, M.M., Ghatrehsamani, S., Akbarzadeh, S.: On the running-in nature of metallic tribo-components: a review. *Wear* **474–475**, 203871 (2021)
- Blau, P.J.: Four great challenges confronting our understanding and modeling of sliding friction research sponsored by the U.S. Department of Energy, assistant secretary for energy efficiency and renewable energy, office of transportation technologies, as part of the heavy vehicle propulsion system materials Program, under contract DE-AC05-96OR22464 with Lockheed Martin energy research corporation. In: Dowson, D., Taylor, C.M., Childs, T.H.C., Dalmaz, G., Berthier, Y., Flamand, L., Georges, J.M., Lubrecht, A.A. (eds.) *Tribology Series*, pp. 117–128. Elsevier, Amsterdam (1998)
- Blau, P.J.: Interpretations of the friction and wear break-in behavior of metals in sliding contact. *Wear* **71**(1), 29–43 (1981)
- Blau, P.J.: How common is the steady-state? The implications of wear transitions for materials selection and design. *Wear* **332–333**, 1120–1128 (2015)
- Lijesh, K.P., Khonsari, M.M.: On the onset of steady state during transient adhesive wear. *Tribol. Int.* **130**, 378–386 (2019)
- Hanief, M., Wani, M.F.: Effect of surface roughness on wear rate during running-in of En31-steel: model and experimental validation. *Mater. Lett.* **176**, 91–93 (2016)
- Blau, P.J.: On the nature of running-in. *Tribol. Int.* **38**(11), 1007–1012 (2005)
- Mezghani, S., Demirci, I., Yousfi, M., El Mansori, M.: Running-in wear modeling of honed surface for combustion engine cylinder liners. *Wear* **302**(1), 1360–1369 (2013)
- Ghatrehsamani, S., Akbarzadeh, S., Khonsari, M.M.: Experimental and numerical study of the running-in wear coefficient during dry sliding contact. *Surf. Topogr. Metrol. Prop.* **9**(1), 015009 (2021)

12. Vojtov, V.A., Biekirov, A.S., Voitov, A.V., Tsymbal, B.M.: Running-in procedures and performance tests for tribosystems. *J. Frict. Wear* **40**(5), 376–383 (2019)
13. Argatov, I.I., Fadin, Y.A.: A Macro-scale approximation for the running-in period. *Tribol. Lett.* **42**(3), 311–317 (2011)
14. Ghatrehsamani, S., Akbarzadeh, S., Khonsari, M.M.: Experimentally verified prediction of friction coefficient and wear rate during running-in dry contact. *Tribol. Int.* **170**, 107508 (2022)
15. Ding, C., Feng, S., Qiao, Z., Zhou, Z., Piao, Z.: Running-in performance of 7075 aluminum alloy strengthened by burnishing technology. *J. Mech. Sci. Technol.* **37**(5), 2545–2553 (2023)
16. Ding, C., Zhu, H., Sun, G., Jiang, Y., Wei, C.: Characteristic parameters and evolution of the running-in attractor. *Int. J. Bifurc. Chaos* **29**(04), 1950044 (2019)
17. Takens, F.: *Detecting Strange Attractors in Turbulence*. Springer, Berlin, Heidelberg (1981)
18. Hsia, F.-C., Elam, F.M., Bonn, D., Weber, B., Franklin, S.E.: Tracing single asperity wear in relation to macroscale friction during running-in. *Tribol. Int.* **162**, 107108 (2021)
19. Zhang, X., Zhang, L., Yu, X., Zhu, X., Tu, Y., Kang, X.: A novel and quantitative determination method for the running-in process through dimensionless real contact area. *Wear* **514–515**, 204554 (2023)
20. Gates, J.D.: Two-body and three-body abrasion: a critical discussion. *Wear* **214**(1), 139–146 (1998)
21. Zambrano, O.A., Muñoz, E.C., Rodríguez, S.A., Coronado, J.J.: Running-in period for the abrasive wear of austenitic steels. *Wear* **452–453**, 203298 (2020)
22. Zambrano, O.A., Aguilar, Y., Valdés, J., Rodríguez, S.A., Coronado, J.J.: Effect of normal load on abrasive wear resistance and wear micromechanisms in FeMnAlC alloy and other austenitic steels. *Wear* **348–349**, 61–68 (2016)
23. Zambrano, O.A.: Stacking fault energy maps of Fe–Mn–Al–C–Si steels: effect of temperature, grain size, and variations in compositions. *J. Eng. Mater. Technol.* (2016). <https://doi.org/10.1115/14033632>
24. Castañeda, J.A., Zambrano, O.A., Alcázar, G.A., Rodríguez, S.A., Coronado, J.J.: Stacking fault energy determination in Fe–Mn–Al–C austenitic steels by X-ray diffraction. *Metals* **11**(11), 1701 (2021)
25. Zambrano, O.A., Castañeda, J.A., Camargo, M. *Towards the comprehension of the stacking fault energy in Fe-Mn-Al-C steels*. in *6th European Conference on Computational Mechanics (ECCM 6) (Solids, Structures and Coupled Problems)*. Glasgow, UK, 2018 International Center for Numerical Methods in Engineering (CIMNE) Barcelona
26. International, A.S.T.M., *G99-17 Standard test method for wear testing with a pin-on-disk apparatus*. West Conshohocken (2006)
27. Queener, C.A., Smith, T.C., Mitchell, W.L.: Transient wear of machine parts. *Wear* **8**(5), 391–400 (1965)
28. Stachowiak, G., Batchelor, A.W.: *Engineering Tribology*. Butterworth-Heinemann, Oxford (2013)
29. Totten, G.E.: *Glossary of terms: Friction, Lubrication, and Wear Technology, Friction Lubrication, and Wear Technology*. ASM International, Almere (2017)
30. Yokohata, T., Kato, K., Miyamoto, T., Kaneko, R.: Load-dependency of friction coefficient between silicon-oxides and diamond under ultra-low contact load. *J. Tribol.* **120**(3), 503–509 (1998)
31. Xu, Z., Shi, X., Zhang, Q., Zhai, W., Li, X., Yao, J., Chen, L., Zhu, Q., Xiaov, Y.: Effect of sliding speed and applied load on dry sliding tribological performance of TiAl matrix self-lubricating composites. *Tribol. Lett.* **55**(3), 393–404 (2014)
32. Zambrano, O.A., Gallardo, K.F., Polania, D.M., Rodríguez, S.A., Coronado, J.J.: The role of the counterbody's oxide on the wear behavior of HSS and Hi-Cr. *Tribol. Lett.* **66**(1), 1 (2017)
33. Sjöberg, S., Sosa, M., Andersson, M., Olofsson, U.: Analysis of efficiency of spur ground gears and the influence of running-in. *Tribol. Int.* **93**, 172–181 (2016)
34. Akbarzadeh, S., Khonsari, M.M.: On the optimization of running-in operating conditions in applications involving EHL line contact. *Wear* **303**(1), 130–137 (2013)
35. Zambrano, O.A.: A general perspective of Fe–Mn–Al–C steels. *J. Mater. Sci.* **53**(20), 14003–14062 (2018)
36. Zambrano, O.A., Valdés, J., Aguilar, Y., Coronado, J.J., Rodríguez, S.A., Logé, R.E.: Hot deformation of a Fe–Mn–Al–C steel susceptible of κ -carbide precipitation. *Mater. Sci. Eng. A* **689**, 269–285 (2017)
37. Zambrano, O.A., Tressia, G., Souza, R.M.: Failure analysis of a crossing rail made of Hadfield steel after severe plastic deformation induced by wheel-rail interaction. *Eng. Fail. Anal.* **115**, 104621 (2020)
38. Gibbs, P.J., Hough, P.D., Thürmer, K., Somerday, B.P., San Marchi, C., Zimmerman, J.A.: Stacking fault energy based alloy screening for hydrogen compatibility. *JOM* **72**(5), 1982–1992 (2020)
39. Rodríguez, J.S., Duran, J.F., Aguilar, Y., Alcazar, G.A.P., Toro, A., Zambrano, O.A.: Effect of Al content on the low-stress abrasive wear behaviour of Fe-18Mn-xAl-07.C alloys. *Tribol. Int.* (2023). <https://doi.org/10.1016/j.triboint.2023.108286>
40. Song, W., Ingendahl, T., Bleck, W.: Control of strain hardening behavior in High-Mn austenitic steels. *Acta Metall. Sin. (Engl. Lett.)* **27**(3), 546–556 (2014)
41. Sun, G., Huang, J., Peng, J., Wu, W.: Effect of strain hardening on wear and corrosion resistance of 316L Austenitic stainless steel. *J. Mater. Eng. Perform.* (2023). <https://doi.org/10.1007/s11665-023-08535-8>

Publisher's Note Springer Nature remains neutral with regard to jurisdictional claims in published maps and institutional affiliations.

Authors and Affiliations

O. A. Zambrano¹ · B. Iglesias-Guerrero² · S. A. Rodríguez² · J. J. Coronado²

✉ O. A. Zambrano
oscar.zambrano@nrc-cnrc.gc.ca

✉ J. J. Coronado
john.coronado@correounivalle.edu.co

¹ Mining Wear and Corrosion Laboratory, National Research Council Canada, 4250 Westbrook Mall, Vancouver, BC V6T 1 W5, Canada

² Research Group of Fatigue and Surfaces, Mechanical Engineering School, Universidad del Valle, Cali, Colombia